

Probing nanoscale photo-oxidation in organic films using spatial hole burning near-field scanning optical microscopy

G. M. Credo, G. M. Lowman, J. A. DeAro, P. J. Carson, D. L. Winn, and S. K. Buratto

Department of Chemistry and Biochemistry, University of California, Santa Barbara, California 93106-9510

(Received 14 December 1999; accepted 1 February 2000)

Spatial hole burning near-field scanning optical microscopy (SHB-NSOM) is used to locally photopattern three species of organic thin films, poly(2-methoxy, 5-(2'-ethyl hexyloxy)-*p*-phenylene vinylene) (MEH-PPV), *tris*-8-hydroxyquinoline aluminum (Alq₃) and dye-functionalized polyelectrolyte self-assembled layers, on a 100 nm length scale. In SHB-NSOM the film is illuminated with light from a stationary NSOM tip to induce photo-oxidation. The reduction in the fluorescence yield resulting from this exposure is then mapped using fluorescence NSOM (FL-NSOM). We have examined the localized photo-oxidation as a function of time, position, and environment free from the limits of far-field spatial averaging. In all of the thin film materials studied we find that the long-time diameter of the dark spot is much larger than the tip diameter and is a signature of energy migration. Characteristic lengths of the energy migration are extracted from this data by a simple diffusion model and are found to be of the order of a few hundred nanometers for each of the films studied. © 2000 American Institute of Physics. [S0021-9606(00)71116-0]

I. INTRODUCTION

Small molecule organic semiconductors and conjugated polymers have been the subject of great interest due to their interesting optical properties and their technological importance.¹⁻⁶ Applications of these materials in light emitting diodes (LEDs), photodiodes and lasers have provided strong motivation for a detailed understanding of the optical and electronic properties. It is also observed that most of these materials are air sensitive and readily undergo photo-oxidation, which lowers the fluorescence quantum yield and degrades the overall performance of the film. Such molecular-based materials are largely amorphous but exhibit a complex morphology containing areas of local order or microcrystallinity with characteristic lengths well below the wavelength of visible light. Virtually all of the optical properties, including photo-oxidation, are dependent on these variations in morphology.⁷⁻¹⁰ In particular, the mobility of electronic excited states, such as excitons and polarons, is strongly dependent on the local structure.¹¹⁻¹³ Traditionally, optical properties of organic films are probed via far-field steady-state or time-resolved spectroscopy which typically have an illumination spot size of greater than one micron. A major caveat of these techniques is that they average over a large area, usually several square microns in size. Since the length scale for variations in morphology is of the order of 10-100 nm, these ensemble measurements are inadequate for an accurate picture of excited-state diffusion in these materials. The approach adopted for the experiments discussed here, however, is to measure the nanoscale optical and optoelectronic properties *directly* by probing the material in a very localized region using near-field optics. In this paper we concentrate on probing nanoscale photo-oxidation, which we show to be dependent on film morphology. In addition, lo-

calized photo-oxidation provides a means for probing excited-state diffusion in these materials.¹⁴⁻¹⁶

This direct approach is made possible by the recent development of near-field scanning optical microscopy (NSOM).¹⁷ Over the past 5 years NSOM has proven to be a powerful tool for mapping the nanoscale optical properties of a variety of thin film materials including conjugated polymers and molecular semiconductors.¹⁸⁻²⁰ In typical experiments, the NSOM tip is used as a passive probe to image the light scattered or emitted by the sample. Early in the development of NSOM, however, it was shown that the NSOM tip could also be used as an active probe to modify the optical properties of thin films by light-induced heating or photochemistry.²¹ Subsequently, several groups have utilized near-field illumination to lithographically pattern commercial photoresists and conjugated polymers with subwavelength spatial resolution.²¹⁻²³ In the experiments discussed in this paper we use the NSOM tip to locally photo-oxidize three species of organic thin films: MEH-PPV, Alq₃ and dye-functionalized polyelectrolyte layers. The photo-oxidation results in a decrease in the fluorescence of the film. A variety of patterns can be produced in this manner all with a feature size dependent on the illuminated spot size and the excited-state diffusion length. The size and shape of the photo-induced pattern is then imaged using fluorescence NSOM (FL-NSOM).²⁴

In cases where the excited-state diffusion length is comparable to or larger than the aperture diameter it is possible to use this photo-patterning experiment to measure excited-state diffusion directly. This is accomplished by first exposing the film in a single spot and subsequently imaging the spot size and shape using fluorescence NSOM. In this technique, known as spatial hole burning NSOM (SHB-NSOM),

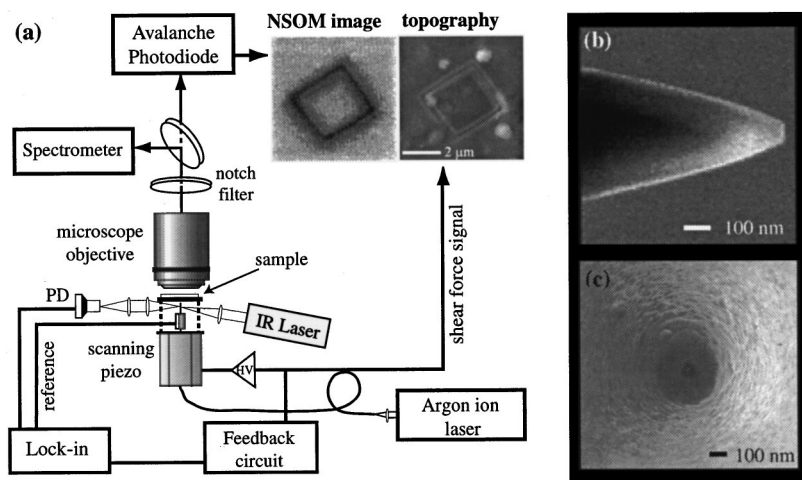


FIG. 1. Schematic of the transmission NSOM experimental configuration (a) and SEM images of an uncoated (b) and coated (c) NSOM tips. The sample is held in the near-field (~ 10 nm) of the NSOM tip via the optical shear force technique. The shear force technique creates simultaneous topography and optical NSOM images. The setup also allows for simultaneous fluorescence spectra to be taken from a localized section of the sample.

the evolution of the photo-oxidized spot size with time is governed by the excited-state diffusion and the photo-oxidation kinetics.^{14–16}

Using a two-dimensional model for excited-state diffusion with continuous irradiation, the steady-state density of excited states $\rho(r)$ is determined from the diffusion equation¹⁶

$$D \left[\frac{\partial^2}{\partial r^2} + \frac{1}{r} \frac{\partial}{\partial r} \right] \rho(r) - \frac{\rho(r)}{\tau} + P e^{4(\ln 2)r^2/\Delta^2} = 0, \quad (1)$$

where D is the excited-state diffusion constant, Δ is the full width at half maximum (FWHM) of the irradiation spot (for a Gaussian profile), P is the rate at which excited-state density is created by the laser at the center of the irradiation spot, and τ is the excited-state lifetime, which is of the order of 1 ns for each of the organic films studied. For $\sqrt{D\tau}$ comparable to or less than Δ , the steady-state excited-state density is dominated by the shape of the irradiation spot. For $\sqrt{D\tau} \gg \Delta$, the steady-state excited-state density takes on long tails with a more exponential character away from the irradiation spot. In SHB-NSOM the shape and size of the photo-oxidation spot is a function of both the excited-state density at each point in the film and the photo-oxidation rate.

It is important to note that in addition to measuring excited-state diffusion, the SHB-NSOM technique provides the means for probing photo-oxidation on a local scale, free from spatial averaging. This advantage is important in order to observe subtle changes in the fluorescence spectrum as a function of exposure time as well as any spatial variation of the photo-oxidation kinetics.

We compare the local photo-oxidation properties of three different organic optical materials, MEH-PPV thin films, Alq₃ thin films and dye-functionalized polyelectrolyte self-assembled layers. Each of these materials undergoes irreversible photo-oxidation, which results in a decrease in the film fluorescence. Each material also has slightly different morphology, which is shown to influence the photochemistry. In MEH-PPV films the film packing density varies on the 100 nm scale resulting in a spatial variation of the photo-oxidation kinetics and the excited-state diffusion length. In addition, the photo-oxidation in MEH-PPV was found to change both the surface morphology of the film as well as

the fluorescence spectrum. In the Alq₃ films, however, the film morphology is much more uniform. As a result, the photochemistry shows very little spatial variation. Few effects are observed in the surface morphology and no changes were observed in the fluorescence spectrum. In dye-functionalized polyelectrolyte layers there were no changes in the surface topography or in the emission spectrum. The photo-oxidation was found to be uniform despite the inherent heterogeneity of the polyelectrolyte films.²⁵

II. EXPERIMENT

The NSOM apparatus used for exposing the organic films is shown in Fig. 1, and has been described in detail elsewhere.²⁶ Near-field excitation is accomplished using a subwavelength aperture that exists at the end of a tapered optical fiber coated with 100 nm of Ag.¹⁷ The tapered fibers are fabricated using a commercial pipette puller with a 10 W CO₂ laser as the heat source. Metallization of the fiber tips is done using thermal evaporation at a base pressure of 2×10^{-6} torr with the tips positioned at a slight angle to shadow the end from the metal source. All of the tips used in our experiments are optimized for throughput of the excitation wavelength, 457.9 nm or 514 nm from an Ar⁺ laser, at a maximum illumination power of 1 kW/cm².

The FL signal is collected with a high numerical aperture (NA=0.85) objective and routed to either an avalanche photodiode (APD) for imaging or to a spectrometer/CCD detector for spectroscopy via the optics of a conventional optical microscope. The excitation wavelength is suppressed with a holographic notch filter. We construct fluorescence images of our samples point-by-point by raster scanning the sample while keeping the tip fixed. The scanner is controlled with commercial scanning probe microscopy electronics (Digital Instruments, Santa Barbara, CA).

The standard optically detected shear force techniques^{27,28} are used to maintain the tip within the near field (~ 15 nm) of the surface of the film [Fig. 1(a)]. This feedback mechanism provides a simultaneous topography image with the FL-NSOM image. The feedback loop, which maintains the tip-sample distance, is also active during the exposure of the patterns as well as during imaging.

SHB-NSOM is performed by programming the scanning electronics so that the NSOM tip traces a specific pattern over the surface of the sample. The photo-oxidation patterns are written using the maximum illumination power possible (1 kW/cm^2) and are imaged using FL-NSOM at lower illumination powers (typically of the order of 100 W/cm^2).

Glass coverslips (Fisher) were used as sample substrates for the MEH-PPV and Alq_3 films. The slides were rinsed in acetone and flamed before use. The MEH-PPV (Uniax Corp.) films were spin cast from a $10 \mu\text{M}$ solution of MEH-PPV in *p* xylene. The resulting thin films had a thickness of approximately 100 nm and a surface roughness below 5 nm as measured with FL-NSOM. Before high power illumination, the FL signal was observed to be uniform to less than 5%, even on the 100 nm length scale.

Alq_3 powdered solids (Aldrich) were purified by train-sublimation. The solid was placed in a baffled tungsten evaporating boat and sublimed at low pressures (5.5×10^{-6} torr, Kurt J. Lesker evaporator). Deposition rate and film thickness were monitored by quartz crystal thickness monitor (Leybold Inficon). The typical deposition rate was 2–5 Å/s. The Alq_3 films in these experiments were between 20 nm and 100 nm thick. Before high power illumination, the FL signal was observed to be uniform to less than 2% and the topography had a root-mean-squared (rms) surface roughness value of <1 nm. The characterization of as-deposited Alq_3 films by NSOM is described in more detail elsewhere.²⁹

Dye-functionalized polyelectrolyte layers were produced via polyelectrolyte self-assembly according to the procedure described by Decher.^{30,31} Poly(sodium *p*-styrenesulfonate) (PSS), was purchased from Acros Organics. Poly(allylamine hydrochloride) (PAH) and Fluorescein Isothiocyanate (FI), were purchased from Aldrich. All materials were used without further purification. PAH was covalently labeled with fluorescein using a procedure previously reported.³² This reaction produced a dye concentration of 1 per 20 monomer units as measured by UV-Vis spectroscopy. This implies that in an idealized straight polymer chain the average distance between fluorescein molecules is approximately 58 Å.

All polyelectrolyte self-assembled films were prepared on microscope cover glass (Fisher, size $25 \times 25 \times \frac{1}{2} \text{ mm}^3$). Ultra-purified (Millipore) water ($\text{pH}=5.5$) was used for all preparation steps. The glass surface was functionalized by immersion in a Piranha solution, $\text{H}_2\text{SO}_4/\text{H}_2\text{O}_2(7:3)$, and sonicated for 1 h and then rinsed with ultra-pure water and dried. Substrates were then sonicated for 1 h in $\text{H}_2\text{O}/\text{H}_2\text{O}_2/\text{NH}_4\text{OH} (5:1:1)$ solution, rinsed and dried. Adsorption of PAH and PSS was carried out in 0.02 M aqueous solution.^{30,31} FI-PAH was adsorbed from a 7 mM solution in ethylene glycol, which was made slightly basic by addition of solid sodium hydroxide. Films were prepared by sequential dipping of the functionalized substrates in the appropriately charged polyelectrolyte solution. Many multilayer film architectures are possible using this method of self-assembly. Typically a single layer of unlabeled PAH (cation), or unlabeled PSS (anion) are deposited by immersion for 15–20 minutes in the polyelectrolyte solution, followed by rinsing

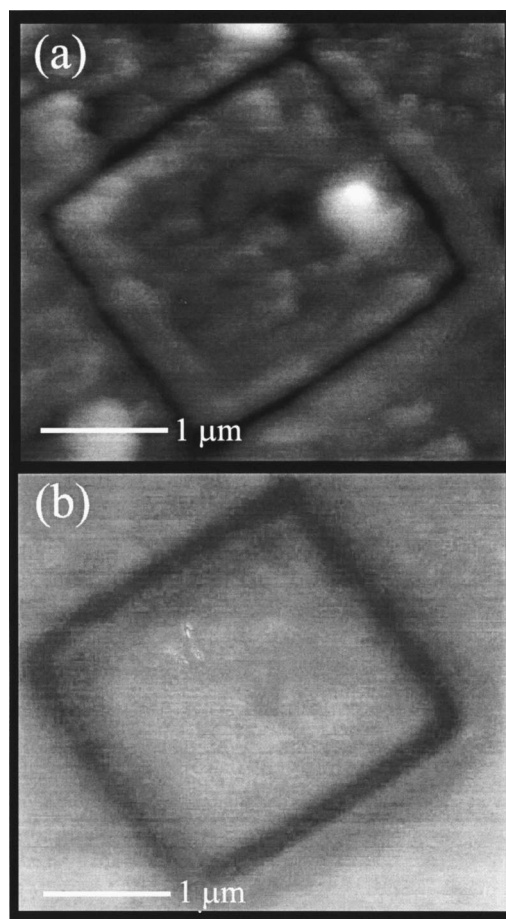


FIG. 2. Photo-oxidation patterning of a thin film of MEH-PPV and photo-induced topography. The diamond pattern in (b) was written in the FL-NSOM image with 10 passes of the NSOM tip, the corresponding topography is shown in (a). The topographical depression is ~ 50 nm deep and the ridges are ~ 25 nm tall. The black to white contrast in (b) is 20%.

with ultra-pure water and drying. Dye-labeled PAH was adsorbed from a 10 minute immersion, rinsed with ethanol/ultra-pure water/ethanol, then dried. Film growth was monitored by UV/Vis spectroscopy.

III. RESULTS AND DISCUSSION

An example of photo-patterning of MEH-PPV is shown in Fig. 2. The rate of exposure of the diamond pattern was $1 \mu\text{m/s}$, which is equivalent to 20 ms per pixel. The diamond pattern was exposed 10 times (a total of 200 ms/pixel) before imaging the resulting fluorescence. Under these conditions a clear photo-pattern is observed with a depth of contrast of 20% and a spatial resolution of 200 nm. In addition, a change in the surface topography is also observed [Fig. 2(a)]. The topography shows both a slight protrusion (15 nm) on each side of the diamond pattern as well as a depression (50 nm) in the middle. This topography is attributed to melting of the polymer film. It is important to note that the melting only occurs from absorption of the excitation light and was not observed in the absence of light or in the presence of light not absorbed by the polymer. We have determined that the onset of the topography occurs for exposure times larger than 30 ms/pixel. In addition, we do not observe a change in the

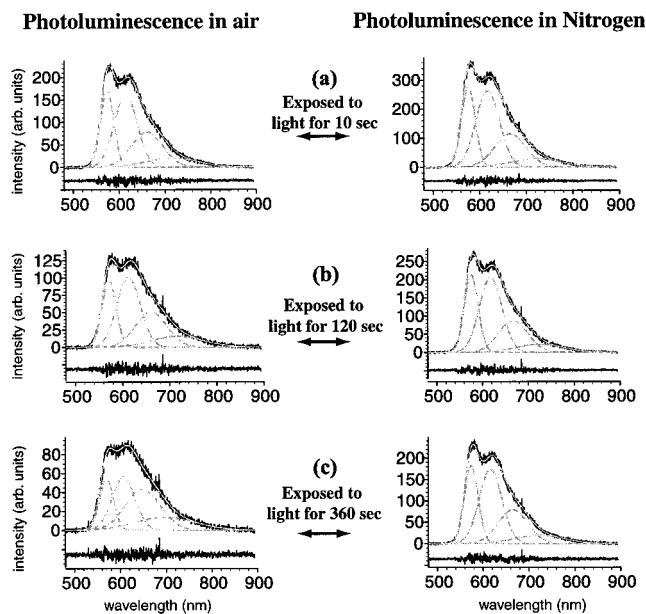


FIG. 3. Fluorescence spectra from a fresh MEH-PPV film in air (left-hand side) and under flowing nitrogen (right-hand side) over time. The fluorescence spectra after 10 s (a), 120 s (b), and 360 s (c) are shown. The spectra are fit to four Gaussians shown in gray with the residual shown below each spectrum. The spectrum changes with exposure time, not only in the overall intensity, but also in the ratio of the second and first vibronic peak.

lateral size of the depression with increased exposure. The only change observed is the height of the protrusion and the depth of the depression which both increase with increased exposure.

A change in the fluorescence spectrum was also observed during the photo-patterning process. This change is illustrated in Figs. 3 and 4. Figure 3 shows the fluorescence spectra from a single spot after 10 s, 120 s, and 360 s of exposure both in air and under flowing nitrogen. Each spectrum was fitted to the sum of four Gaussians, as shown in light gray, with a single energy defining the splitting between adjacent peaks during the fit. Figure 4 shows a plot of the ratio of the height of the second peak to the height of the first peak as a function of exposure time (the widths of these two

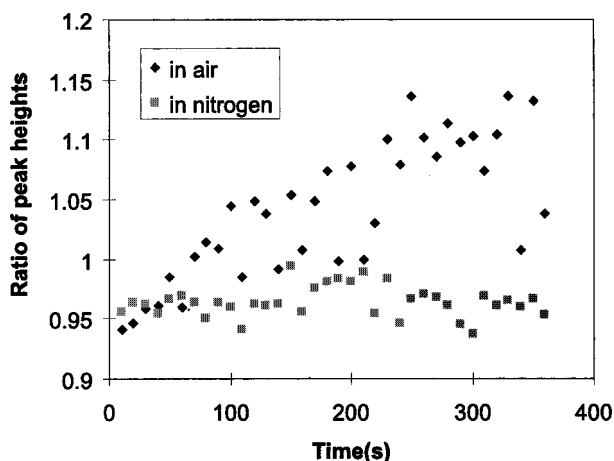


FIG. 4. The change in the ratio of the intensities of the second to first vibronic bands of the fluorescence spectra over time for samples of a fresh MEH-PPV thin film in air (♦) and nitrogen (■).

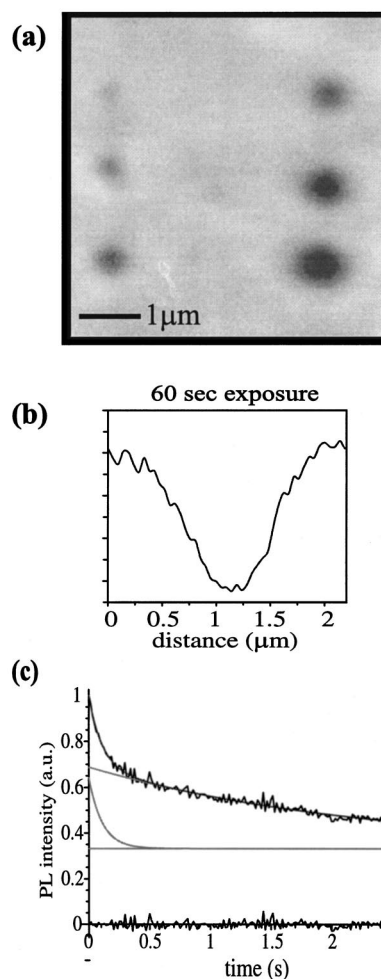


FIG. 5. Spatial hole burning of a thin film of MEH-PPV. The FL-NSOM image (a) shows the result of varying the exposure time of a single location to the light from the NSOM tip. The first column of holes were made with 5 s, 10 s, and 15 s exposures and the second column were made with 30 s, 40 s, and 60 s exposures. As the exposure time increases, the fluorescence intensity decreases and the size of the affected area, measured by the FWHM of the dark spot, increases. The line cut in (b) shows the hole profile for the 60 s hole. The graph in (c) shows the decrease in the fluorescence signal as a function of exposure time. A double exponential fit to the data is shown in gray with the overall decay. The residual is shown along the bottom of the graph.

peaks is nominally constant). As is seen from both figures the change in the fluorescence spectrum as a function of exposure time in air is characterized by an increase in the intensity of the second vibronic band relative to the first vibronic band. A slight blue shift in air relative to nitrogen is also observed, with the blueshift increasing with exposure time. It is also important to note that the changes in the fluorescence spectrum observed in air are drastically reduced under flowing nitrogen (also shown in Figs. 3 and 4). These changes are attributed to additional, unresolved vibronic coupling to carbonyl groups formed during photo-oxidation of the polymer.^{33,34} The production of carbonyls in PPV derivatives during exposure to light and oxygen has been observed previously in spatially averaged experiments using IR spectroscopy.³⁵ In these experiments, however, very little change in the fluorescence spectrum was observed. We believe this is due to spatial-averaging that results from a large

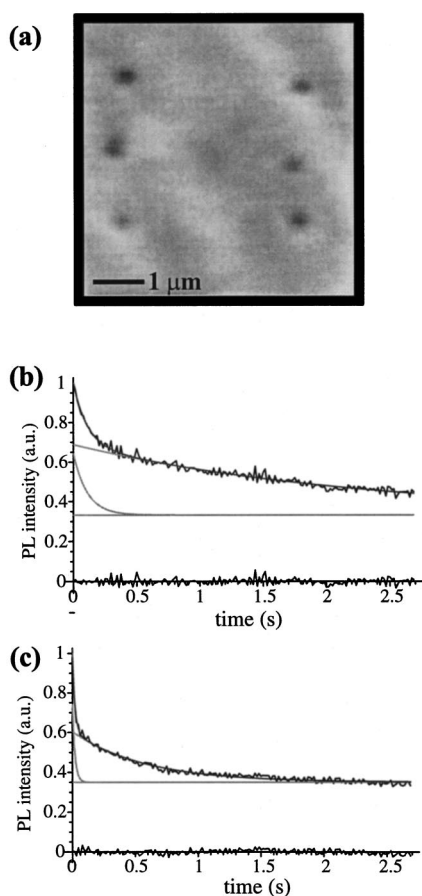


FIG. 6. SHB-NSOM of MEH-PPV as a function of position. The FL-NSOM image (a) shows the affect of exposing the film in various locations for the same amount of time (5 s). The two fluorescence decays shown in (b) and (c) are from the middle hole on the right and the top left hole, respectively. The fluorescence decays have been fit to two exponentials and an offset. For (b) the decay time constants were $\tau_1=0.109$ s and $\tau_2=5$ s and the decay time constants for (c) were $\tau_1=0.02$ ms and $\tau_2=1$ s.

excitation spot size and nonuniform photo-oxidation of the polymer film. This nonuniformity is probed further in the SHB-NSOM experiments discussed below.

The results of SHB-NSOM on a 100 nm thick MEH-PPV film are presented in Figs. 5 and 6. Figure 5 shows an array of six dark spots created by exposing the film over a single spot for exposure times from 5 s to 60 s. As is clearly observed in the image of Fig. 5(a) the diameter of the dark spot increases and the fluorescence signal decreases with increasing exposure time. Figure 5(b) shows a one-dimensional line trace of the fluorescence intensity of the 60 s hole. Figure 5(c) shows the fluorescence yield decay as a function of exposure time at the center of a hole. A multiexponential fit to the transient of Fig. 5(c) shows that this data fits well to the sum of two exponentials with time constants of 0.8 s and 14 s. These time constants represent the kinetics of the photo-oxidation. The fast time constant is attributed to the surface photo-oxidation and the slow time constant is attributed to the subsurface photo-oxidation, which is limited by diffusion of the oxygen into the bulk of the film. It is important to note that films left out in air for more than a few hours exhibit nearly single exponential photo-oxidation kinetics with a time constant of the order of 0.5–5 s.

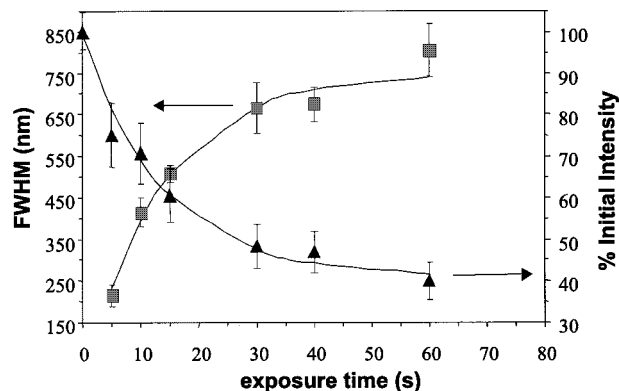


FIG. 7. Parameters of a SHB-NSOM experiment on a 100 nm thick MEH-PPV film. The graph shows the decrease in the percent of the percent initial intensity (\blacktriangle) of each hole, as well as the broadening of the hole diameter (\blacksquare) with increasing exposure time. At zero exposure time the fluorescence signal is 100%. The decay of the fluorescence signal and the rise of the dark spot diameter both fit to a single exponential with a time constant of 14 s. The fit for each data set is shown as a solid line through the points.

The photo-oxidation kinetics are extremely sensitive to the position on the films as illustrated by the data of Fig. 6. In this experiment the film is exposed for 5 s over six different spots on the film. As is observed in the data of Fig. 6, the fast time constant varies from 0.02 s to 0.2 s and the slow time constant varies from 1 s to 10 s. This variation is attributed to different packing density of the MEH-PPV film, which is known to vary on the 100 nm length scale. It is also important to note that the order of magnitude variation in the photo-oxidation kinetics is much larger than the 5% variation of the film fluorescence, which implies higher sensitivity of the photo-oxidation to film morphology than the film fluorescence.

Another important observation regarding the data of Figs. 5 and 6 is the large size of the dark spot after 60 s of exposure. Although the illumination spot is only 100 nm in diameter, the dark spot reaches a pseudo-steady-state size of nearly 1 μ m. This is indicative of excited-state diffusion. Figure 7 shows a plot of both the fractional decrease (measured at the center of the spot) and diameter of the spot as a function of exposure time. The change in diameter with exposure time and the decrease in fluorescence intensity approach a pseudo-asymptote at 60 s. Both curves fit well to a single exponential with a time constant of 15 s, which is approximately equal to that obtained for the slow time constant in the fit to the data of Fig. 5(c). This is expected since the evolution of the diameter of the dark spot is indicative of the photo-oxidation kinetics. Since the data of Fig. 7 was acquired with a 5 s time resolution, the fast time constant (of the order of 100 ms) was not observed due to insufficient data points at early times. Considering the diffusion model discussed in Eq. (1), the shape of the photo-oxidation hole extrapolated to zero time should match the inverted shape of the steady-state excited-state density peak. For our conditions the FWHM of this peak roughly corresponds to diffusion length. Extrapolation of the width in Fig. 7 to zero time puts a rough upper bound (since we may be missing fast kinetics) on the diffusion length of 50 nm.

This value is consistent with exciton diffusion lengths in

MEH-PPV reported by several groups to be of the order of 10–100 nm.^{35–37} We considered the possibility that the large size of the dark spot is due to scattering of the light from the near-field tip within the film. We do not believe the scattering would account for such a large diameter of the dark spot since most of the light is confined to and is absorbed within one aperture diameter due to the highly localized nature of the evanescent near-field radiation.³⁸ It is apparent that the large width of the photo-oxidation hole at longer times is primarily due to the effect of saturating the photo-oxidation directly under the excitation source. It is also possible that the photo-oxidation process itself, which alters both the chemical identity of the polymer film as well as its morphology, influences the shape of the photo-oxidation hole. The introduction of carbonyl groups into PPV films has been shown to enhance the photoconductivity implying a higher mobility for photocarriers in an oxidized film. This would also increase the steady-state size of the dark spot if these photocarriers also contribute to photo-oxidation.

As mentioned earlier, we have observed changes in MEH-PPV fluorescence spectra in oxygenated air which are more pronounced than when the sample was scanned in nitrogen.³⁸ Both oxygen which has diffused into the sample bulk and oxygen present in the air can react with MEH-PPV to form carbonyl groups. In both cases, triplet oxygen present in the film may contribute to the observed energy migration in MEH-PPV films.

The localized photo-oxidation of Alq₃ thin films is presented in Figs. 8, 9, and 10. As in the photo-oxidation of MEH-PPV films, the effects of SHB-NSOM on a 100 nm thick vacuum-deposited Alq₃ film results in a dark spot and the diameter of the dark spot increases with increasing exposure time as is observed in Fig. 8(a). A one-dimensional line trace of the 60 s dark spot is shown in Fig. 8(b). The decrease in fluorescence intensity fits well to a single Lorentzian, which is a good approximation of the shape expected. The fluorescence yield decay is shown in Fig. 8(c), which fits well to a multiexponential decay with time constants of 5 s, 31 s, and 205 s. As with the MEH-PPV films, the fast time constant is attributed to surface photo-oxidation while the slow time constants are attributed to oxidation of the bulk. In contrast to the photo-oxidation of MEH-PPV, however, no heterogeneity of the SHB-NSOM was observed in the photo-oxidation of Alq₃ films as seen in Fig. 9. The fluorescence yield decays for each of the four spots are equivalent with the same photo-oxidation time constants. In addition, the shape of the fluorescence spectrum [Fig. 9(b)] does not change as a function of exposure time, only the fluorescence signal changes. This is not surprising since the morphology of Alq₃ films is much more uniform than that of MEH-PPV. We also note that very little change in topography is observed in the photo-oxidation of Alq₃. The only effects observed in the topography after exposure occurred for very thin films <30 nm thick. Thus, the heating induced by absorption in 100 nm thick Alq₃ films is much less than that observed in MEH-PPV films.

Figure 10 shows a plot of the diameter of the dark spot and the decrease in fluorescence as a function of exposure time. The hole depth fits well to a sum of two exponentials

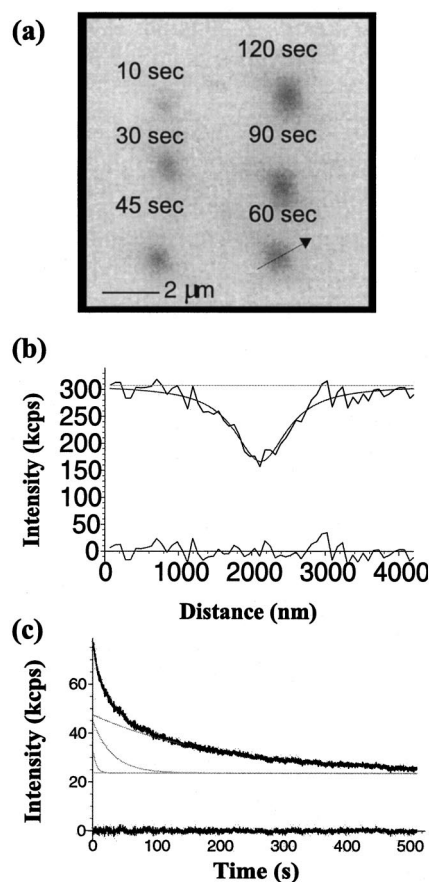


FIG. 8. SHB-NSOM of a 100 nm thick Alq₃ film. The FL-NSOM image (a) shows the results of varying the exposure time of a single location to the light from the NSOM tip for various lengths of time, as marked: 10 s, 30 s, 45 s, 60 s, 90 s, and 20 s. The line cut in (b) shows the profile of the 60 s hole in (a). Graph (c) is a representative time course for a 100 nm Alq₃ film. Fitting this curve to three decaying exponentials we obtained time constants of $\tau_1 = 5$ s, $\tau_2 = 31$ s, and $\tau_3 = 205$ s. The residual is shown along the bottom of the graph.

with time constants of 52 s and 203 s which agrees well with the fit to the data of Fig. 8(c) for the photo-oxidation kinetics. The fast time constant was not obtainable from this data due to lack of data points for early exposure times. The exponential rise of the dark spot diameter required only a single exponential to fit the data with a time constant of 360 s. This suggests that the evolution of the dark spot diameter is not limited to the photo-oxidation kinetics, but is also dependent on another long-time process such as the slow diffusion of oxygen ions or diffusion of deeply trapped carriers. Deeply trapped carriers in Alq₃ films have been reported in previous studies.^{39,40} Extrapolation of the hole width to zero time provides a rough upper bound on the diffusion length for energy migration in Alq₃ determined from the data of Fig. 10 of 400 nm; approximately a 10-fold increase over the largest exciton diffusion length reported in the literature for Alq₃.^{41,42}

As in the case of MEH-PPV, the photo-oxidation of Alq₃ results in the formation of new chemical species. According to studies on the hydrolytic stability of Alq₃, the primary product of this photo-oxidation is a dark nonemissive polymer resulting from the polymerization of freed

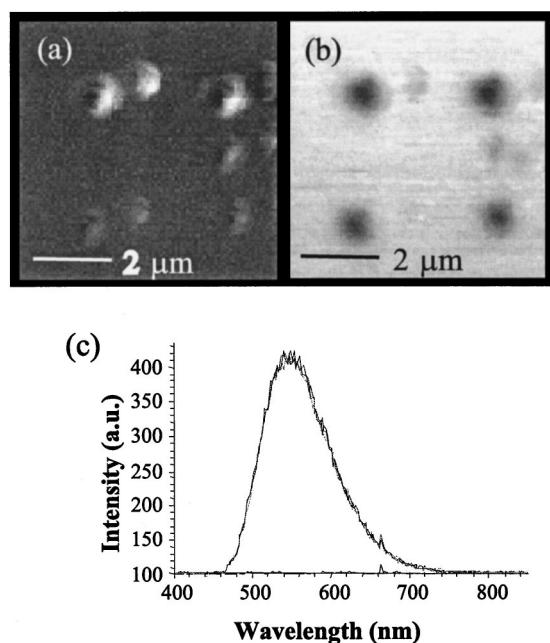


FIG. 9. SHB-NSOM of a 20 nm Alq_3 film as a function of position. The shear force topography image (a) contains four depressions, with raised edges, that correspond to four separate 20 s exposures to the NSOM tip. The FL-NSOM image (b) taken simultaneously with (a) reveals decreased fluorescence efficiency at the four areas exposed to the NSOM tip. Identical fluorescence spectra (c) were obtained for each exposed spot. The shape of these spectra are characteristic of the rest of the film, but the fluorescence intensity is less than surrounding regions of the film.

8-hydroxyquinoline.^{43,44} While the exact structure of this polymer has yet to be determined, the polymer has been shown to be an acceptor for efficient energy transfer from Alq_3 .⁴³ If this energy transfer is sufficiently long range or there are a number of cascading energy transfer pathways, then it is possible that this dark polymer could quench Alq_3 over very long distances.^{43,45}

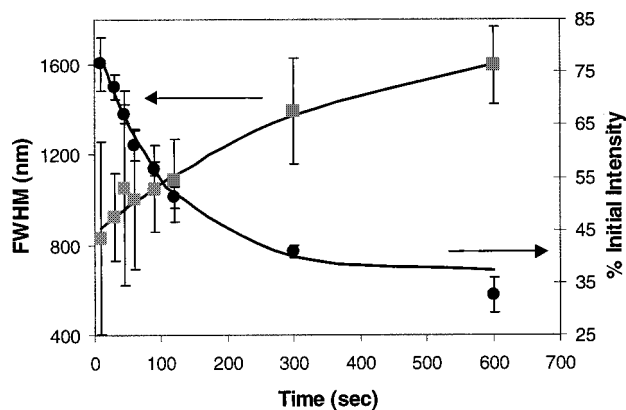


FIG. 10. Parameters of a SHB-NSOM experiment on a 100 nm thick Alq film. The graph shows the decrease in the % initial intensity (●) from each hole, as well as the broadening of the hole diameter (■) with increasing exposure time. The width has been fit to a single rising exponential with $\tau = 360$ s. The fluorescence intensity decreases with time and has been fit to two decaying exponentials with $\tau_1 = 53$ s and $\tau_2 = 205$ s. These time constants compare favorably to the time constants obtained from the fluorescence yield decay of Fig. 8(c).

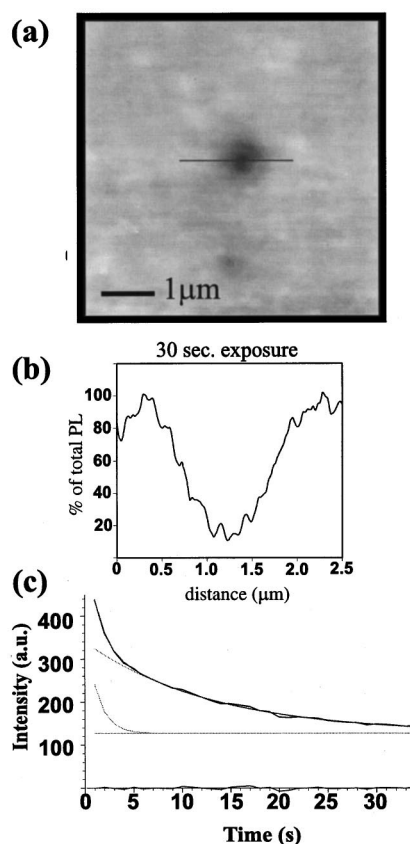


FIG. 11. SHB-NSOM of a 50 nm thick self-assembled film of PSS/FI-PAH (nine bilayers). FL-NSOM image (a) following 30 s exposure to the stationary NSOM tip. Line cut (b) of the hole in fluorescence image (a) as marked. The graph in (c) shows the decrease in the fluorescence signal as a function of exposure time. The resulting signal was fit to two exponentials and an offset, with $\tau_1 = 1.3$ s and $\tau_2 = 11.3$ s.

Finally, we have examined photo-oxidation and energy migration in self-assembled films of PSS/FI-PAH (nine bilayers). Unlike the organic semiconductors MEH-PPV and Alq_3 , this film does not produce delocalized excited states. Energy migration in these materials will occur via homomolecular energy transfer,⁴⁶⁻⁴⁸ which depends strongly on the concentration of dye molecules in the film. The localized photo-oxidation of a 50 nm self-assembled PSS/FI-PAH film (nine bilayers) is presented in Figs. 11 and 12. Figure 11(a) shows the result of an SHB-NSOM dark spot after 30 s exposure. Like MEH-PPV and Alq_3 , the diameter of the dark spot increases and the fluorescence signal decreases with increasing exposure time (see Fig. 12). Figure 11(b) shows a one-dimensional line trace of the hole in the fluorescence image of Fig. 11(a). Figure 11(c) shows the fluorescence yield decay that fits well to a multiexponential with time constants of 1.3 s and 11.3 s. We also observe no heterogeneity of the photo-oxidation on the 100 nm length scale nor do we observe any change in the fluorescence spectrum as a function of exposure time.

The increase of the diameter of the dark spot and the corresponding decrease in fluorescence yield is presented in Fig. 12(a). Both curves are fit well to two exponentials with time constants approximately equal to the time constants observed for the photo-oxidation kinetics [Fig. 11(c)]. Extrapo-

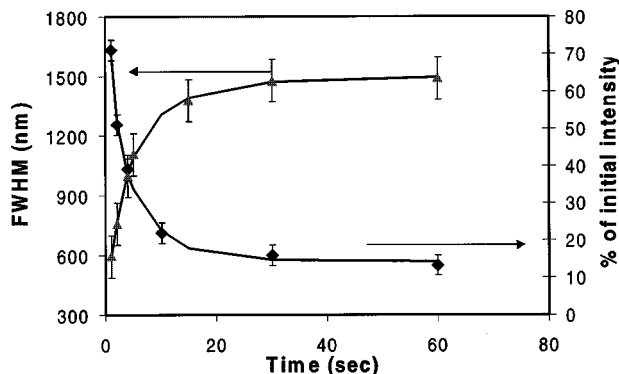


FIG. 12. Parameters of a SHB-NSOM experiment on a 50 nm thick PSS/Fl-PAH film. The graph shows the decrease in the % initial intensity (◆) from each hole, as well as the broadening of the hole diameter (▲) with increasing exposure time. At zero exposure time the fluorescence signal is 100%. The decay of the fluorescence signal was fit to two exponentials with $\tau_1=0.8$ s and $\tau_2=6.0$ s. The rise of the dark spot diameter was fit to two exponentials with time constants of $\tau_1=1.3$ s and $\tau_2=11.3$ s.

lating the width in Fig. 12 to zero time gives a rough upper bound of the diffusion length for energy migration of 200 nm. While this is a large diffusion length it is not unexpected for these materials. The loading of the fluorescein dye was determined to be 1:20, which implies that the average distance between dye molecules is 58 Å in an idealized straight polymer chain. Since the polymer film is an ensemble of disordered polymer chains a conservative estimate of this distance is 0.5 times the Förster radius R_0 (58.2 Å) for energy transfer. Since the rate of energy transfer scales as $(R_0/R)^6$ where R is the distance between neighboring fluorescein molecules, the energy can be transferred up to 64 times in one excited-state lifetime (1 ns). This would imply a diffusion length of many hundreds of nanometer as is observed in our data. Furthermore, reduction of the concentration of dye molecules should drastically reduce the diffusion length, which has been observed in other experiments (not shown).

IV. CONCLUSIONS

We have shown that SHB-NSOM can be applied to a number of luminescent organic films to produce nanoscale photo-patterns, probe photochemistry on a 10–100 nm scale and to determine the characteristic length of excited-state diffusion. In the molecular semiconductors (MEH-PPV and Alq₃) the excited-state diffusion observed in our experiments are several times larger than previously reported values. We suggest that the large diffusion lengths may be due to chemical and topological changes in the film which alters the energy migration. We also observe long range diffusion in dye-functionalized polyelectrolyte layers which is attributed to efficient homomolecular energy transfer. In addition, our experiments revealed a number of interesting differences in the local photo-oxidation properties of the three films studied. MEH-PPV was the most readily photo-oxidized and showed a strong heterogeneity of the photo-oxidation, which could be correlated to film morphology. In addition, the surface topography of the photo-oxidized region indicated localized heating and melting of the polymer film. Changes in the

vibronic bands of the fluorescence spectrum were also observed upon exposure to light. These properties were shown to have a strong heterogeneity attributed to changes in the packing density of the film. These same signatures of photo-oxidation were not observed in the Alq₃ films or the dye-functionalized polyelectrolyte films.

ACKNOWLEDGMENTS

We would like to thank the Heeger group (Physics, UCSB, CA) and Uniax Corp. (Santa Barbara, CA) for assistance with sample preparation of MEH-PPV, and the Thompson group (Chemistry, USC, CA) for assistance with sample preparation of Alq₃. This work was supported by the David and Lucile Packard Foundation, the NSF Nanotechnology Initiative and the Alfred P. Sloan Foundation.

- ¹J. R. Sheats *et al.*, *Science* **273**, 884 (1996).
- ²L. J. Rothberg and A. J. Lovinger, *J. Mater. Res.* **11**, 3174 (1996).
- ³C. W. Tang and S. A. VanSlyke, *Appl. Phys. Lett.* **51**, 913 (1987).
- ⁴J. H. Burroughes *et al.*, *Nature (London)* **347**, 539 (1990).
- ⁵G. Gustafsson *et al.*, *Nature (London)* **357**, 477 (1992).
- ⁶N. C. Greenham, S. C. Moratti, D. D. C. Bradley, R. H. Friend, and A. B. Holmes, *Nature (London)* **365**, 628 (1993).
- ⁷D. A. Halliday *et al.*, *Adv. Mater.* **5**, 40 (1993).
- ⁸J. H. Butler, D. C. Joy, G. F. Bradley, and S. J. Krause, *Polymer* **36**, 1781 (1995).
- ⁹R. L. Miller and R. F. Boyer, *J. Polym. Sci.* **22**, 2043 (1984).
- ¹⁰J. Kerimo, D. M. Adams, P. F. Barbara, D. M. Kaschak, and T. Mallouk, *J. Phys. Chem. B* **102**, 9451 (1998).
- ¹¹J. R. Sheats, Y.-L. Chang, D. B. Roitman, and A. Stocking, *Acc. Chem. Res.* **32**, 193 (1999).
- ¹²J. J. M. Halls, K. Pichler, R. H. Friend, S. C. Moratti, and A. B. Holmes, *Appl. Phys. Lett.* **68**, 3120 (1996).
- ¹³S. V. Rakhmanova and E. M. Conwell, *Appl. Phys. Lett.* **75**, 1518 (1999).
- ¹⁴V. M. Kenkre and Y. M. Wong, *Phys. Rev. B* **22**, 5716 (1980).
- ¹⁵V. M. Kenkre, P. E. Parris, and D. Schmid, *Phys. Rev. B* **32**, 4946 (1985).
- ¹⁶W. Heller, A. Filoramo, P. Roussignol, and U. Bockelmann, *Solid-State Electron.* **40**, 725–728 (1996).
- ¹⁷E. Betzig, J. K. Trautman, T. D. Harris, J. S. Weiner, and R. L. Kostelak, *Science* **251**, 1468–1470 (1991).
- ¹⁸R. C. Dunn, *Chem. Rev.* **99**, 2891 (1999).
- ¹⁹S. K. Buratto, *Curr. Opin. Solid State Mater. Sci.* **1**, 485 (1996).
- ²⁰D. A. VandenBout, J. Kerimo, D. A. Higgins, and P. F. Barbara, *Acc. Chem. Res.* **30**, 204 (1997).
- ²¹E. Betzig and J. K. Trautman, *Science* **257**, 189 (1992).
- ²²I. I. Smolyaninov, D. L. Mazzoni, and C. L. Mazzoni, *Appl. Phys. Lett.* **67**, 3859 (1995).
- ²³P. K. Wei, J. H. Hsu, B. R. Hsieh, and W. S. Fann, *Adv. Mater.* **8**, 573 (1996).
- ²⁴R. S. Berry, S. A. Rice, and J. Ross, in *Physical Chemistry* (Wiley, New York, 1980), pp. 720.
- ²⁵G. Decher, *Science* **277**, 1232 (1997).
- ²⁶K. D. Weston, J. A. DeAro, and S. K. Buratto, *Rev. Sci. Instrum.* **67**, 2924 (1996).
- ²⁷E. Betzig, P. L. Finn, and J. S. Weiner, *Appl. Phys. Lett.* **60**, 2484 (1992).
- ²⁸R. Toledo-Crow, P. C. Yang, Y. Chen, and M. Vaeziravani, *Appl. Phys. Lett.* **60**, 2957 (1992).
- ²⁹G. M. Credo and S. K. Buratto, *Adv. Mater.* **12**, 183 (2000).
- ³⁰J. D. Hong and G. Decher, *Makromol. Chem., Macromol. Symp.* **46**, 321 (1991).
- ³¹J. D. Hong, J. Schmitt, and G. Decher, *Thin Solid Films* **210/211**, 831 (1992).
- ³²D. M. Kaschak and T. E. Mallouk, *J. Am. Chem. Soc.* **118**, 4222 (1996).
- ³³D. G. J. Sutherland *et al.*, *Appl. Phys. Lett.* **68**, 2046 (1996).
- ³⁴G. D. Hale, S. J. Oldenburg, and N. J. Halas, *Appl. Phys. Lett.* **71**, 1483 (1997).
- ³⁵J. C. Scott *et al.*, *J. Appl. Phys.* **79**, 2745 (1996).

- ³⁶D. Vacar, E. S. Maniloff, D. W. McBranch, and A. J. Heeger, *Phys. Rev. B* **56**, 4573 (1997).
- ³⁷M. Yan, L. J. Rothberg, F. Papadimitrakopoulos, M. E. Galvin, and T. M. Miller, *Phys. Rev. Lett.* **73**, 744 (1994).
- ³⁸J. A. DeAro and S. K. Buratto (unpublished).
- ³⁹P. E. Burrows *et al.*, *J. Appl. Phys.* **79**, 7991 (1996).
- ⁴⁰E. W. Forsythe, D. C. Morton, C. W. Tang, and Y. Gao, *Appl. Phys. Lett.* **73**, 1457 (1998).
- ⁴¹P. E. Burrows and S. R. Forrest, *Appl. Phys. Lett.* **64**, 2285 (1994).
- ⁴²C. W. Tang, S. A. VanSlyke, and C. H. Chen, *Appl. Phys. Lett.* **65**, 3610 (1989).
- ⁴³F. Papadimitrakopoulos, X. M. Zhang, D. L. Thomsen, and K. A. Higginson, *Chem. Mater.* **8**, 1363 (1996).
- ⁴⁴F. Papadimitrakopoulos, X. M. Zhang, and K. A. Higginson, *IEEE J. Sel. Top. Quantum Electron.* **4**, 49 (1998).
- ⁴⁵R. Priestley, I. Sokolik, A. D. Walser, C. W. Tang, and R. Dorsinville, *Synth. Met.* **84**, 915 (1997).
- ⁴⁶L. W. Runnels and S. F. Scarlata, *Biophys. J.* **69**, 1569 (1995).
- ⁴⁷P. J. Sims and T. Wiedmer, *Biochemistry* **23**, 3260 (1984).
- ⁴⁸L. Song, E. J. Hennink, I. T. Young, and H. J. Tanke, *Biophys. J.* **68**, 2588 (1995).